

Journal of Materials Chemistry A

Accepted Manuscript



This is an *Accepted Manuscript*, which has been through the Royal Society of Chemistry peer review process and has been accepted for publication.

Accepted Manuscripts are published online shortly after acceptance, before technical editing, formatting and proof reading. Using this free service, authors can make their results available to the community, in citable form, before we publish the edited article. We will replace this *Accepted Manuscript* with the edited and formatted *Advance Article* as soon as it is available.

You can find more information about *Accepted Manuscripts* in the [Information for Authors](#).

Please note that technical editing may introduce minor changes to the text and/or graphics, which may alter content. The journal's standard [Terms & Conditions](#) and the [Ethical guidelines](#) still apply. In no event shall the Royal Society of Chemistry be held responsible for any errors or omissions in this *Accepted Manuscript* or any consequences arising from the use of any information it contains.

Li-ion conductivity in $\text{Li}_9\text{S}_3\text{N}$

Lincoln J. Miara¹, Naoki Suzuki², William D. Richards³, Yan E. Wang³, Jae Chul Kim³, Gerbrand Ceder^{3,4}

¹Samsung Advanced Institute of Technology – USA, 255 Main St., Suite 702, Cambridge, MA 02142

²Samsung R&D Institute Japan—Mino Semba Center Bldg. 13F, 2-1-11, Semba Nish Minoh, Osaka 562-0036, Japan

³Department of Materials Science and Engineering, Massachusetts Institute of Technology, 77 Massachusetts Ave, Cambridge, MA 02139

⁴Department of Materials Science & Engineering, UC Berkeley, 210 Hearst Mining Building, Berkeley, CA 94720-1760

Keywords

$\text{Li}_9\text{S}_3\text{N}$, solid state electrolyte, lithium metal barrier coating, DFT.

Abstract

$\text{Li}_9\text{S}_3\text{N}$ (LSN) is investigated as a new lithium ion conductor and barrier coating between an electrolyte and Li metal anode in all solid state lithium ion batteries. LSN is an intriguing material since it has a 3-dimensional conduction channel, high lithium content, and is expected to be stable against lithium metal. The conductivity of LSN is measured with impedance spectroscopy as $8.3 \times 10^{-7} \text{ S cm}^{-1}$ at room temperature with an activation energy of 0.52 eV. Cyclic voltammetry (CV) scans showed reversible Li plating and stripping. First principles calculations of stability, nudged elastic band (NEB) calculations, and ab initio molecular dynamics (AIMD) simulations support these experimental results. Substitution as a means to enhance conductivity is also investigated. First-principles calculations predict that divalent cation substituents displace a lithium from a tetrahedral site along the migration pathway, and reduce the migration energy for the lithium ions in the vicinity of the substituent. A percolating path with low migration energies (~ 0.3 eV) can be formed throughout the crystal structure at a concentration of $\text{Li}_{8.5}\text{M}_{0.25}\text{S}_3\text{N}$ ($\text{M} = \text{Ca}^{2+}$, Zn^{2+} , or Mg^{2+}), resulting in predicted conductivities as high as $\sigma_{300\text{K}} = 2.3 \text{ mS cm}^{-1}$ at this concentration. However, the enhanced conductivity comes at the expense of relatively large substitution energy. Halide substitution, such as Cl on a S site (Cl_S^\bullet in Kröger-Vink notation), has a relatively low energy cost, but only provides a modest improvement in conductivity.

Introduction

The safety problems associated with conventional lithium ion batteries are largely related to electrolyte decomposition. One approach to address this problem is to replace the current liquid electrolyte with inorganic solids. A solid electrolyte must have high lithium ion conductivity, as well as chemical and electrochemical compatibility with the electrodes; however, decades of research have yet to discover a commercially viable replacement for organic liquid electrolytes. A promising technique is to use a combination of solid materials instead of a single material. For example, thin films of LiPON or LiBH_4/LiI have been used to form a barrier layer to protect the lithium metal anode,^{1,2} while LiNbO_3 or Li_3BO_3 have been employed as protective coatings on the cathode side.^{3,4} Paired with a highly conductive separator, a bi- or tri-layer electrolyte offers a method to meet the intense demands on a solid electrolyte.

To find a lithium ion conducting anode barrier coating, stable towards reduction against lithium metal, we searched ternary materials made from two binary compounds which are both stable against Li metal, since this new material is also expected to be stable against lithium.⁵ Li_2S and Li_3N , both stable against Li metal, combine to form the recently synthesized anti-fluorite compound $\text{Li}_9\text{S}_3\text{N}$ (LSN).⁶ The structure has high lithium content, the starting components are inexpensive, the synthesis route is relatively simple, and like most sulfides, we find the final material is soft and easy to mix with other battery components. Therefore, this material is an interesting candidate for a lithium metal protective layer in all solid state batteries.

In a recent publication the contribution of the anion framework towards lithium ion mobility was examined.⁷ In that work it was shown that the FCC anion framework has a higher intrinsic migration barrier as compared to the BCC framework. The connecting tetrahedral sites in a bcc sulfur framework allow Li to diffuse with only small coordination changes along the path leading to a migration barrier as low as 0.15 eV. FCC and HCP anion frameworks, on the other hand, have an inherently large migration barrier (> 0.5 eV at typical lattice volumes) as the pathway in FCC structures is composed of a face-sharing tetrahedral-octahedral-tetrahedral network. The octahedral site is higher in energy for Li, requiring a large activation barrier for an ion to pass through this site. The difficulty for ion mobility in these structures is demonstrated in Li_2S in which the S ions form an FCC sublattice and shows an experimental activation energy of 0.74 eV.⁸

LSN is formed by substituting one of the four sulfur sites in the unit-cell of Li_2S with N and charge compensating with an extra lithium, as shown in figure 1. Like Li_2S , LSN also has a perfect FCC anion sublattice, but unlike Li_2S it has an extra lithium atom in an octahedral site. It is expected that this extra

lithium may reduce the large tetrahedral-octahedral site energy difference, lowering the activation energy compared with Li_2S . To further reduce the activation energy, we examine the possibility of substituting other atoms into the structure to significantly modify the energy landscape. In this work, we investigate the structural and phase stability of LSN, synthesize and measure its conductivity, identify substitutions with the lowest incorporation energy, and identify mechanisms for improving conductivity using first principles calculations.

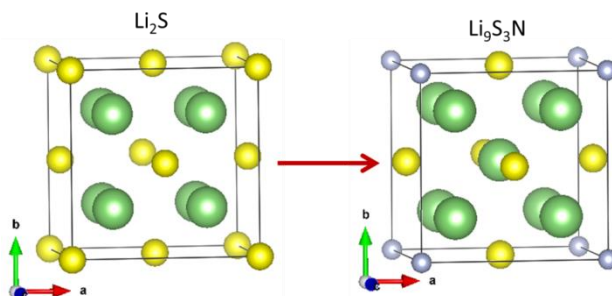


Figure 1: LSN is formed by substituting one S site in Li_2S with N and charge compensating with a Li at the 6 sulfur coordinated octahedral site; LSN has an anti-fluorite crystal structure with an FCC anion sublattice.

Methods

Computation

All Density Functional Theory (DFT) calculations were performed in the Perdew-Burke-Ernzerhof (PBE) generalized-gradient approximation (GGA),⁹ implemented in the Vienna Ab initio Simulation Package (VASP).¹⁰ The projector augmented-wave (PAW)¹¹ method is used for representation of core states. An energy cutoff of 520 eV and a k -point density of at least 1000 per number of atoms in the unit cell were used for total energy calculations. The initial structure was obtained from the Inorganic Crystal Structure Database (ICSD).¹² The stability of LSN against the anode and cathode were calculated by evaluating the potentials of Li at which the compound decomposes, following the methods of reference.¹³

Migration barriers were calculated using the NEB method¹⁴ in a large supercell comprised of $2 \times 2 \times 2$ conventional unit cells to minimize the interaction between the periodic images. A $2 \times 2 \times 2$ k -point grid was used and the cutoff of the kinetic energy was set to 520 eV for all NEB calculations.

The effect of temperature on diffusivity and conductivity were investigated with AIMD simulations implemented in VASP. The computational cost was kept to a reasonable level by using a minimal Γ -centered $1 \times 1 \times 1$ k -point grid, a plane wave energy cut-off of 400 eV, and non-spin-polarized calculations. A supercell containing $2 \times 2 \times 2$ conventional unit cells was used. The initial positions and unit cell volumes were obtained from the DFT relaxation calculations. The Verlet algorithm, as implemented

in VASP, was used to solve Newton's equation of motion. The AIMD time step was 2 fs and the simulation was run for at least 200 ps to ensure convergence. The diffusivity (D) was obtained by performing a linear fitting of the MSD vs. $2dt$. Simulations were carried out at temperatures between 600 to 1000 K to determine the activation energy from Arrhenius plots.¹⁵ The room temperature conductivities (σ) were determined by extrapolation to room temperature and relating the diffusivity to conductivity by the Nernst-Einstein equation: $\sigma = \frac{DNq^2}{kT}$, where N is the carrier density, q the carrier charge, T is the absolute temperature, and k is the Boltzmann constant.

The Li-ion probability density (IPD) was calculated from the AIMD atom trajectories at 800 K. The IPD values within a structure were calculated by assigning the position of each atom during each time step and then applying a Gaussian filter to smooth the results. The total ionic probability density is $\int_{\Omega} P_i = N/\Omega$, where N is the number of Li ions in the unit-cell and the Ω is the volume of the unit-cell.

To find the most stable substituents for vacancy generation, structures with all possible substituents were generated by placing a supervalent ion on the Li-site, or subvalent ion on the S- or N-site and then charge balancing the structure by creating lithium vacancies. The structures were then relaxed with DFT. The most favorable substituents were determined based on thermodynamic considerations. This is determined by checking against all possible linear combinations of compounds in the ICSD in the compositional space, and can be evaluated by the convex hull construction.¹⁶ This construction effectively calculates the driving force for the substituent to precipitate out into one or more secondary phases. The analysis requires the energy of all known compounds in the ternary or quaternary Li-S-N-M (M = substituent) phase diagram. The substituted energies are calculated as:

$$E_{\text{substituent}} = E_{\text{pure}} - E_{\text{substituted}} + \sum_i^N \Delta n_i \mu_i$$

Where $E_{\text{substituted}}$ and E_{pure} are the total energy of the supercell with and without the substituent respectively, Δn_i is the number of atoms of element i added to (or removed from) the supercell to create and charge balance the supercell, and μ_i is the chemical potential of element i . This is summed for all elements (N) which are added or removed during the substitution reaction. The chemical potentials for each element i are determined from the multi-phase equilibrium that contains the composition of the substituted structure. The software suite *pymatgen* is used to generate the phase diagram and calculate the chemical potentials of the elements added or removed during the reaction.¹⁷

Experimental procedure

The starting compounds Li_2S (99.9% Alfa Aesar) and Li_3N (99.5% Strem Chemicals) were mixed with 50% excess Li_3N by weight, and mechanically milled for 1000 min at a rotating speed of 400 rpm using a planetary ball mill (Fritsch Pulverisette 7) with a ZrO_2 pot and ZrO_2 balls. The mixed compound was placed in a boron nitride crucible and sealed in an evacuated quartz tube. This assembly was heated to 600 °C for 24 h in a muffle furnace and slowly cooled to room temperature. The purity of the phase was checked with XRD using an X-ray diffractometer (PANalytical, EMPYREAN) with $\text{Cu-K}\alpha$ radiation. In order to obtain structural parameters, Rietveld refinement was performed using HighScore Plus software.

The electrochemical impedance spectroscopy was measured with an impedance spectrometer (Autolab, FRA32M) between 1 MHz and 10 mHz. For this measurement, a blocking electrode setup was made by sandwiching the LSN powder between two 0.05 mm thick indium foil electrodes and contained in the test cell comprising of a stainless steel outer casing with a Teflon insulator.¹⁸ The powder was pressed to 400 MPa into a pellet of 1.3 cm diameter and ~1 mm thickness. After making an LSN pellet, it was sandwiched between two indium foils and pressed to 100 MPa.

The CV was measured with an AUTOLAB PGSTATM101 controlled by a personal computer at a scan rate of 10 mV s^{-1} . Due to the modest conductivity of the LSN material, we examined the electrochemical stability as follows: first we prepared amorphous Li_3PS_4 (a-LPS), which is known to be stable between 0 and 5 V (vs. Li) during a CV scan by ball-milling a mixture of Li_2S and P_2S_5 with a 3:1 molar ratio. Next, we mixed LSN and the a-LPS in a 1:1 (w/w) ratio and used it as the working electrode. A 0.1 mm thick lithium foil was used for the counter and reference electrodes, and the a-LPS was used as a solid electrolyte separator. These components were assembled in the above mentioned test cell. 200 g of a-LPS was pressed to 40 MPa, and 15 g of W.E. and the lithium foil (C.E.) were affixed to each side of the pellet. The assemblage was pressed to 400 MPa.

All test cells were fabricated in an Ar-filled glove box due to the sensitivity of LSN to moisture. Each test cell was sealed in a laminated bag with Ar gas, and removed from the glove box for the measurements.

Results and Discussion

LSN

The experimental XRD results of LSN are shown in figure 2. All peaks of LSN are observed, and only very minor peaks due to Li_2S are seen. Scale factor, lattice constants, profile parameters, isotropic temperature coefficients, site occupancy factors, atomic coordinates were refined step-by-step to obtain the best fit. Site occupancy factors and atomic coordinates for Li were not refined. Also, it should

be noted that anisotropic temperature factors could not be refined due to the resolution of the lab XRD. The lattice constant of $\text{Li}_9\text{S}_3\text{N}$ is 5.5253 Å, which is almost identical to that in Ref. 6 (5.5151 Å). Atomic distances are also similar: $d(\text{Li-N}) = 2.07211$ Å (1x), $d(\text{Li-S}) = 2.5175$ Å (3x), $d(\text{Li-S}) = 2.76263$ Å (6x). These results are summarized in table 1.

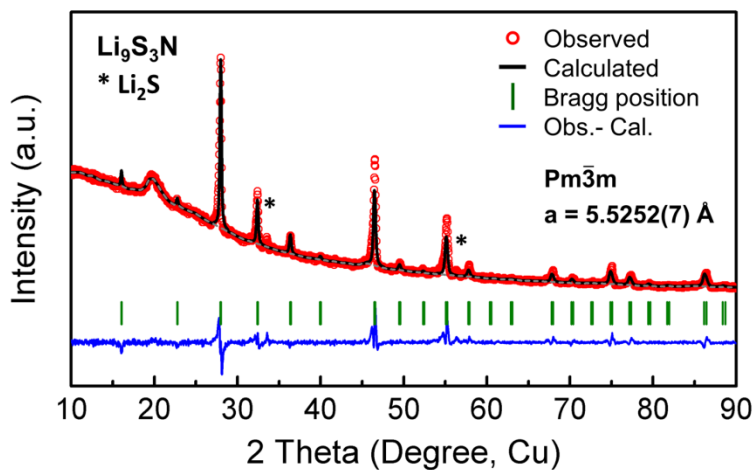


Figure 2: Rietveld refined XRD pattern obtained from $\text{Li}_9\text{S}_3\text{N}$. Fitting agreement indices are $R_p = 4.69$, $R_{wp} = 7.40$, and $\chi^2 = 9.65$ (Pseudo-Voigt fit).

Table 1: Refinement results compared to calculations and prior reference.

$\text{Li}_9\text{S}_3\text{N}$ Samples	Lattice constant (Å)	Volume (Å ³)	$d(\text{Li-N})$ (1x) (Å)	$d(\text{Li-S})$ (3x) (Å)	$d(\text{Li-S})$ (6x) (Å)
Calculated	5.51664	167.8711	2.06883	2.51346	2.75822
Refined	5.52527	168.6788	2.07211	2.5175	2.76263
Ref. 6	5.51513	167.7518	2.09	2.50	2.76

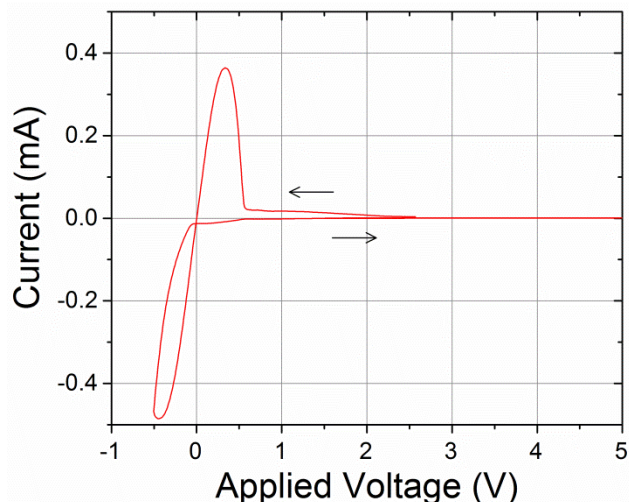


Figure 3: CV performed with a 10 mV s^{-1} scan rate. Li plating and stripping occurs, a small reduction peak is evident at about 0.5 V, but no further reaction is seen out to 5 V.

The electrochemical window of LSN was measured with CV. At a 10 mV s^{-1} scan rate, figure 3, lithium plating and stripping is seen. At about 0.5 V a small reduction peak is observed, but then no further reaction is seen out to 5 V. The small peak at 0.5 V likely corresponds to the decomposition of Li_3N . It has been shown that at a voltage of 0.45 V vs. Li, Li_3N forms N_2 .¹⁹ However, with the loss of nitrogen, it is likely that Li_2S forms a passivation layer, as was shown to occur in thio-phosphate materials in previous DFT studies.²⁰ This passivation layer extends the anodic stability out to about 2 V before Li_2S reduction occurs.^{21,22} Beyond 2 V in the CV scan, it is likely that a surface insulating layer of sulfur prevents further reaction.

The conductivity results measured with EIS are shown in figure 4. The room temperature conductivity was estimated to be $8.3 \times 10^{-7} \text{ S cm}^{-1}$, and the activation energy was 0.52 eV. We attempted to extract a second semicircle related to grain boundaries using the equivalent circuit shown in the inset of figure 4; however, no evidence of a grain boundary contribution was evident even at -10°C . It is possible that the presence of Li_2S lowers the measured impedance, but the amount (based on XRD results) is exceedingly low and the impedance results are likely dominated by LSN.

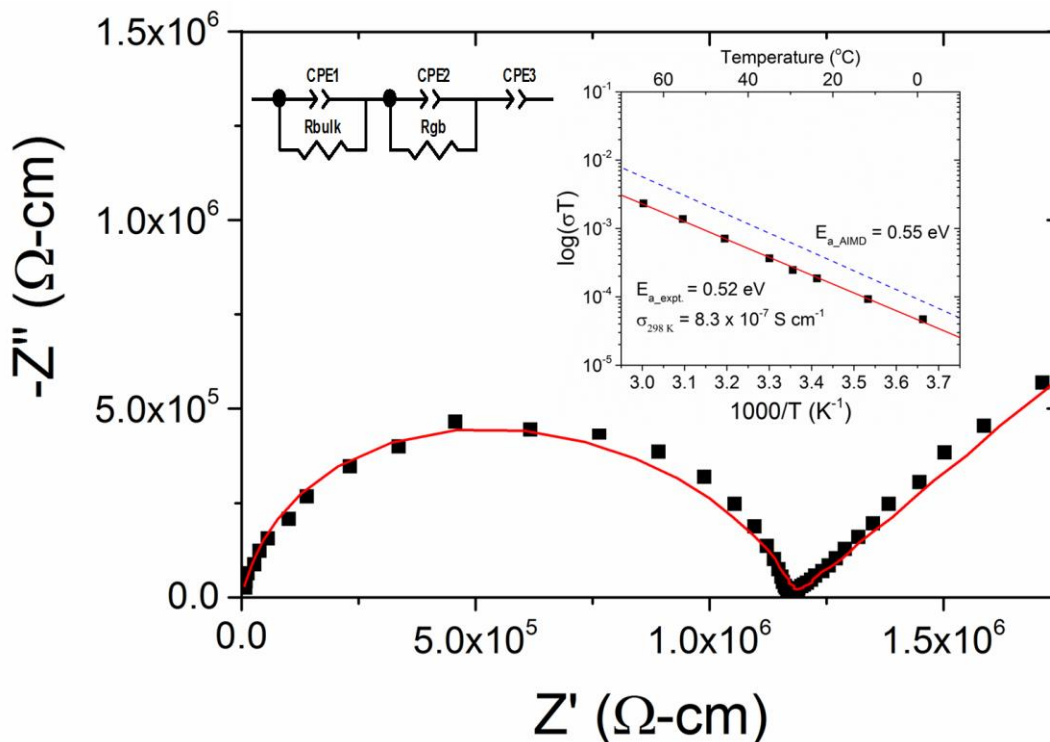


Figure 4: Nyquist plot of the EIS results at 25°C . The conductivity was extracted from the inset equivalent circuit. Results from other temperatures are plotted as an Arrhenius plot in the inset; the blue dashed line is AIMD simulation results for comparison.

To understand the origin of the lithium ion conductivity and diffusivity in LSN, NEB and AIMD simulations were performed. The calculated migration barrier from NEB calculations for one Li vacancy and compensated by a uniform background charge is 0.5 eV (figure 5). For bulk type solid electrolytes this value is relatively high (compare to 0.21 eV for $\text{Li}_{10}\text{GeP}_2\text{S}_{12}$, 0.2 eV for agyroditite-type sulfides, or 0.34 eV for $\text{Li}_7\text{La}_3\text{Zr}_2\text{O}_{12}$ ^{23–26}). In this system it is not possible to stabilize a cation vacancy in the tetrahedral site since it will move to the octahedral site upon geometry relaxation as confirmed in the DFT calculation. The vacancies are relatively stable in the octahedral site coordinated by 6 sulfur atoms (as compared to the tetrahedral vacancies). The lowest energy path for the vacancy to migrate to the neighboring octahedral site is through two neighboring tetrahedral sites, figure 5. In the low vacancy limit, a highly coordinated lithium migration is required involving three moving lithium ions with a migration barrier of 0.5 eV . This barrier is mainly due to the energy of the Li passing through the triangular face shared between the tetrahedral and octahedral sites, and partly from the S- and N-bonds between the two tetrahedral sites, figure S1. Another pathway exists through the octahedral site coordinated by 4 sulfur and 2 nitrogen atoms. This pathway only requires a two atom coordinated motion; however, the migration barrier in this path is about 0.8 eV , figure S2. AIMD calculations were performed on a structure with a single vacancy charge compensated with a positive charge background.

The activation energy is calculated to be 0.55 eV (figure 4) and the room temperature conductivity is extrapolated as $2.4 \times 10^{-6} \text{ S cm}^{-1}$ (table 2). This is in excellent agreement with the conductivity measured experimentally.

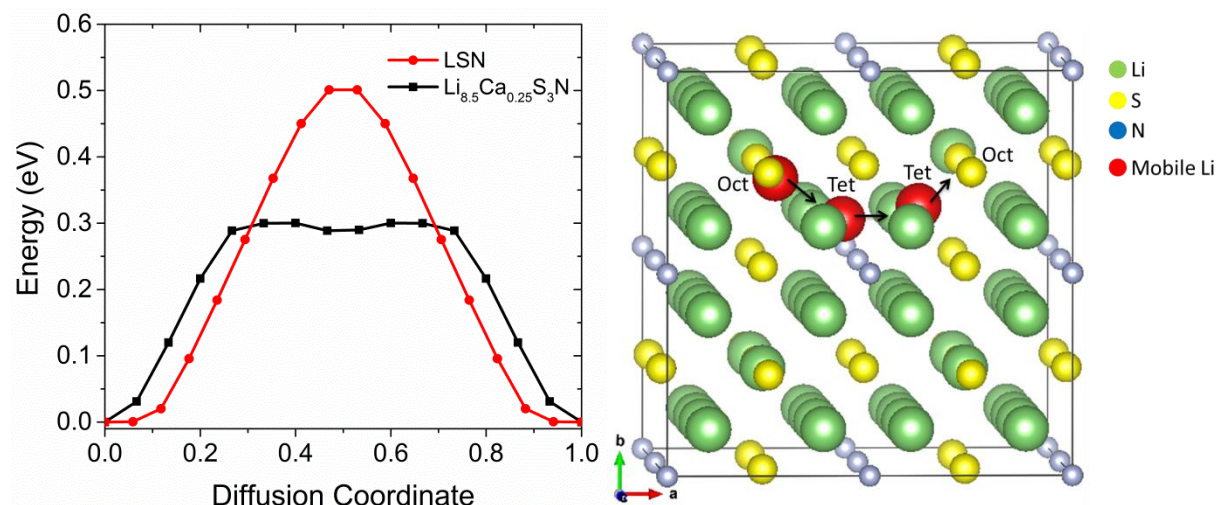


Figure 5: (left) Calculated NEB barrier for vacancy migration along oct-tet-tet-oct pathway with and without Ca. (right) Oct.-tet.-tet.-oct. migration pathway identified from NEB calculations. A coordinated three lithium movement is required.

Table 2: Comparison of calculated and experimental results from LSN

	NEB (eV)	E_a -AIMD (eV)	E_a -Expt. (eV)	$\sigma_{300\text{K}}$ -AIMD (S/cm)	$\sigma_{300\text{K}}$ -Expt. (S/cm)
LSN	0.5	0.55	0.52	2.4×10^{-6}	8.3×10^{-7}

Outlook to Improve Conductivity of LSN

LSN is an attractive material for an anode barrier layer due to its stability against lithium metal; however, its conductivity is too low for use as an electrolyte in a bulk type solid state battery. We investigated the possibility of substituting the material to improve the conductivity.

Using first principles methods, we computed the energy of all possible non-transition metal substituents that create lithium vacancies including S-on-N substitution. The 20 lowest energy substituents are shown in table 3. The most stable substituents are Cl_S^\bullet and Br_S^\bullet on the sulfur sites. The energy for Cl_S^\bullet substitution is only 115 meV per substituent, and is an attractive means for producing vacancies in the LSN material. The lowest energy cation substituents are divalent cations on the Li-site (M_{Li}^\bullet). Ca_{Li}^\bullet is the lowest with a substitution energy of 848 meV per substituent. In all of these structures the lowest energy lithium vacancies reside in the octahedral sites, close to the substituent. Ca and Zn prefer the tetrahedral site, with one nearest Li atom displaced away from the center of the neighboring tetrahedral site towards the octahedral site (figure S1). This displacement moves the Li along the migration pathway and places it in the triangular face between the tetrahedral and octahedral sites.

Based on the results in table 3, we evaluated the effect of Cl_S^\bullet and Ca_{Li}^\bullet substitution for improved conductivity using first principles methods. We created substituted structures with 1-, 2-, and 5- substituents in the 8 formula unit supercell by substituting with Cl and Ca, and charge compensating with lithium vacancies.

The AIMD results are shown in figure 6. The vacancies created by Cl_S^\bullet have a modest effect on conductivity. The activation energy is reduced from 0.53 eV to 0.44 eV and room temperature conductivity improves an order of magnitude to $5.9 \times 10^{-5} \text{ S cm}^{-1}$ (table 4). This value is considerably better than LiPON, and, considering the low substitution energy, may be an attractive means to improve conductivity.

Table 3: Stability of substituents in the LSN structure

Substituent (Kröger-Vink)	Chemical formula	$E_{\text{substitute}}$ (eV/substituent)	Volume (\AA^3)	Density (g/cc)
-	$\text{Li}_{72}\text{S}_{24}\text{N}_8$	-	1333.61	1.71
Cl_S^\bullet	$\text{Li}_{71}\text{S}_{23}\text{N}_8\text{Cl}$	0.115	1341.79	1.71
Br_S^\bullet	$\text{Li}_{71}\text{S}_{23}\text{BrN}_8$	0.33	1348.51	1.75
S_N^\bullet	$\text{Li}_{71}\text{S}_{25}\text{N}_7$	0.452	1365.32	1.69
I_S^\bullet	$\text{Li}_{71}\text{S}_{23}\text{IN}_8$	0.528	1356.85	1.8
Ca_{Li}^\bullet	$\text{Li}_{70}\text{CaS}_{24}\text{N}_8$	0.848	1358.04	1.72
Zn_{Li}^\bullet	$\text{Li}_{70}\text{ZnS}_{24}\text{N}_8$	0.908	1339.69	1.78
F_S^\bullet	$\text{Li}_{71}\text{S}_{23}\text{N}_8\text{F}$	0.974	1330.59	1.7
Mg_{Li}^\bullet	$\text{Li}_{70}\text{MgS}_{24}\text{N}_8$	0.985	1343.53	1.72
$Br_N^{\bullet\bullet}$	$\text{Li}_{70}\text{S}_{24}\text{BrN}_7$	1.188	1372.28	1.73
Cd_{Li}^\bullet	$\text{Li}_{70}\text{CdS}_{24}\text{N}_8$	1.254	1351.83	1.82
Sr_{Li}^\bullet	$\text{Li}_{70}\text{SrS}_{24}\text{N}_8$	1.501	1369.7	1.76
$IN^{\bullet\bullet}$	$\text{Li}_{70}\text{S}_{24}\text{IN}_7$	1.681	1386.36	1.77
$In_{Li}^{\bullet\bullet}$	$\text{Li}_{69}\text{InS}_{24}\text{N}_8$	1.848	1347.53	1.82
$La_{Li}^{\bullet\bullet}$	$\text{Li}_{69}\text{LaS}_{24}\text{N}_8$	1.938	1363.72	1.83
$Be_{Li}^{\bullet\bullet}$	$\text{Li}_{70}\text{BeS}_{24}\text{N}_8$	2.299	1330.11	1.72
$Ba_{Li}^{\bullet\bullet}$	$\text{Li}_{70}\text{BaS}_{24}\text{N}_8$	2.363	1382.5	1.81
$Y_{Li}^{\bullet\bullet}$	$\text{Li}_{69}\text{YS}_{24}\text{N}_8$	2.415	1354.18	1.78
$Sc_{Li}^{\bullet\bullet}$	$\text{Li}_{69}\text{ScS}_{24}\text{N}_8$	2.668	1343.49	1.74
$Ga_{Li}^{\bullet\bullet}$	$\text{Li}_{69}\text{GaS}_{24}\text{N}_8$	2.858	1338.81	1.77
$Ge_{Li}^{\bullet\bullet\bullet}$	$\text{Li}_{68}\text{GeS}_{24}\text{N}_8$	3.057	1335.33	1.77
$Al_{Li}^{\bullet\bullet}$	$\text{Li}_{69}\text{AlS}_{24}\text{N}_8$	3.575	1334.96	1.73

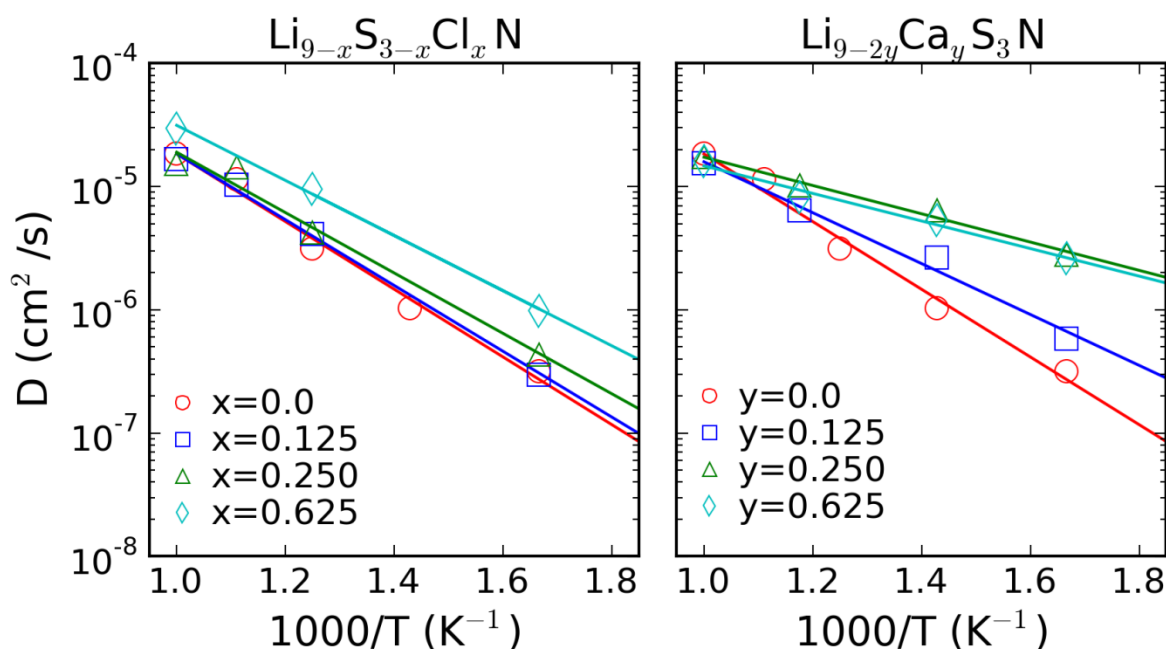


Figure 6: AIMD simulation results; left, Cl- and; right, Ca-substituted LSN. The Cl has limited effect on diffusivity while Ca-substitution beyond $y = 0.25$ shows a rapid diffusivity and little change with further substitution.

Table 4: Summary of AIMD results for Ca and Cl substituted LSN.

		E_a (eV)	σ_{300} (S cm ⁻¹)
Li ₉ S ₃ N		0.545	2.35×10^{-6}
Li _{9-x} S _{3-x} Cl _x N	x		
	0.125	0.530	3.57×10^{-6}
	0.250	0.486	1.18×10^{-5}
	0.625	0.444	5.90×10^{-5}
Li _{9-2y} Ca _y S ₃ N	y		
	0.125	0.409	7.76×10^{-5}
	0.250	0.295	2.27×10^{-3}
	0.625	0.268	9.64×10^{-3}

From figure 6 it is clear that Ca substitution can improve the conductivity significantly. The AIMD simulation results shown in figure 6 indicate that the activation energy decreases from 0.41 eV to 0.27 eV as Ca substitution is increased from 0.125 Ca per formula unit (pfu) to 0.625 Ca pfu. The latter of which would make Ca-substituted LSN a superionic conductor with a room temperature conductivity predicted to be nearly 10 mS cm^{-1} , table 4. The substitution energy for Ca_{Li}^{\bullet} is $0.848 \text{ eV atom}^{-1}$, which is considerably higher than Cl_{S}^{\bullet} . This suggests that synthesis of the highly substituted compounds may be

difficult and would tend to form LiCaN, Li₃N, and Li₂S, requiring a highly non-equilibrium synthesis method to obtain these materials.

We performed NEB calculations on the Li_{8.5}Ca_{0.25}S₃N structure to understand the origin of the improved conductivity in this material. The low energy migration pathway follows the same 3-Li atom coordinated oct-tet-tet-oct pathway as LSN, but the movement occurs in sites adjacent to the Ca (figure S1). The migration barrier is 300 meV (figure 5). The presence of the Ca displaces the lithium along the migration pathway and thus the higher energy of the equilibrium site reduces the barrier to pass through the triangular face.

For further insight we examined the trajectories of the AIMD simulations, figure 7. In the non-substituted structure there is little movement of the Li atoms. As vacancies are created, a few atoms migrate as evidenced by the trajectories of the heavily Cl-substituted Li_{8.375}S_{2.375}Cl_{0.625}N shown in figure 7. For Ca substitution, the AIMD results, figure 6, show a large improvement (30X) in room temperature conductivity as the concentration of Ca changes from 0.125 to 0.25 pfu, whereas the improvement is much smaller between 0.25 and 0.625 Ca pfu (4X). The marked decrease in activation energy between the 0.125 and 0.25 Ca-pfu structures can be explained by examining the probability density. In figure 7, it is seen that the lithium away from the Ca substituents are relatively immobile with the highest probabilities in their ground state locations; however, in the vicinity of the Ca atoms, the situation changes. The probability density is nearly continuous in the oct-tet-tet-oct pathway around the Ca atoms. Furthermore, at Li_{8.5}Ca_{0.25}S₃N a 3-dimensional conduction channel is formed from the connection of the migration pathway between adjacent Ca forming a percolation network. This explains the large improvement in conductivity seen when going from 0.125 to 0.25 Ca-pfu.

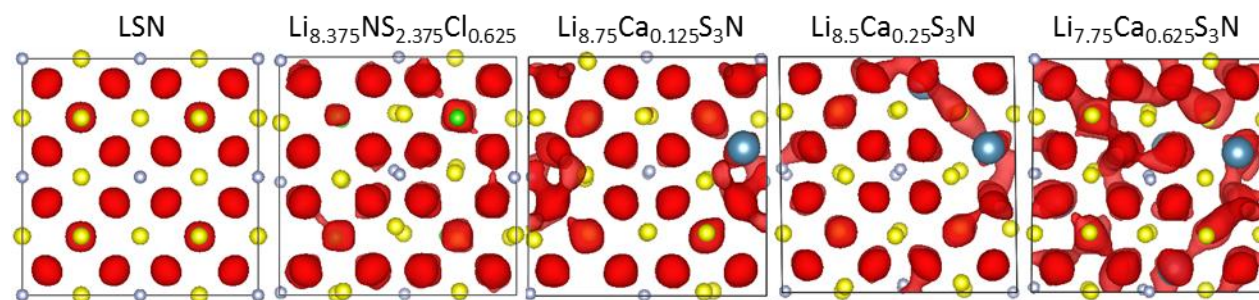


Figure 7: Isosurfaces of the ionic probability density determined from 800 K AIMD simulations.

Conclusions

In this work we studied $\text{Li}_9\text{S}_3\text{N}$, with and without substituents, as a potential anode barrier layer for all solid-state batteries. LSN is attractive since our results show it is stable against lithium metal. LSN was synthesized and shows an ionic conductivity of $8.3 \times 10^{-7} \text{ S cm}^{-1}$ at room temperature with an activation energy of 0.52 eV, in excellent agreement with NEB and AIMD calculations. We explored the possibility of improving conductivity through aliovalent substitution. Cl_S^\bullet substitution was found to have a low incorporation energy, and marginally improves conductivity. $\text{Ca}_{\text{Li}}^\bullet$ substitution to a concentration of $\text{Li}_{8.5}\text{Ca}_{0.25}\text{S}_3\text{N}$ leads to a very high percolated conductivity, but at a cost of high incorporation energy. LSN has the potential to be a cheap anode barrier layer for use in all solid state batteries.

References

- (1) Bates, J.; Dudney, N.; Gruzalski, G.; Zuhr, R. Electrical Properties of Amorphous Lithium Electrolyte Thin Films. *Solid State Ionics* **1992**, *56*, 647–654.
- (2) Sahu, G.; Lin, Z.; Li, J.; Liu, Z.; Dudney, N.; Liang, C. Air-Stable, High-Conduction Solid Electrolytes of Arsenic-Substituted Li_4SnS_4 . *Energy Environ. Sci.* **2014**, *7* (3), 1053.
- (3) Ohta, N.; Takada, K.; Sakaguchi, I.; Zhang, L.; Ma, R.; Fukuda, K.; Osada, M.; Sasaki, T. LiNbO_3 -Coated LiCoO_2 as Cathode Material for All Solid-State Lithium Secondary Batteries. *Electrochem. commun.* **2007**, *9* (7), 1486–1490.
- (4) Jinlian, L.; Xianming, W. U.; Shang, C.; Jiaben, C.; Zeqiang, H. Enhanced High Temperature Performance of LiMn_2O_4 Coated with Li_3BO_3 Solid Electrolyte. *Bull. Mater. Sci.* **2013**, *36* (4), 687–691.
- (5) Neudecker, B. J.; Weppner, W. $\text{Li}_9\text{SiAlO}_8$: A Lithium Ion Electrolyte for Voltages above 5.4 V. *J. Electrochem. Soc.* **1996**, *143* (7), 2198.
- (6) Marx, R.; Lissner, F.; Schleid, T. Li_9NS_3 : Das Erste Nitridsulfid Der Alkalimetalle in Einer Li_2O -Typ-Variante. *Zeitschrift für Anorg. und Allg. Chemie* **2006**, *632* (12-13), 2151–2151.
- (7) Wang, Y.; Richards, W. D.; Ong, S. P.; Miara, L. J.; Kim, J. C.; Mo, Y.; Ceder, G. Design Principles for Solid-State Lithium Superionic Conductors. *Nat. Mater.* **2015**, *advance on*.
- (8) Lin, Z.; Liu, Z.; Dudney, N. J.; Liang, C. Lithium Superionic Sulfide Cathode for All-Solid Lithium–Sulfur Batteries. *ACS Nano* **2013**, *7* (3), 2829–2833.
- (9) Perdew, J. P.; Burke, K.; Ernzerhof, M. Generalized Gradient Approximation Made Simple. *Phys. Rev. Lett.* **1996**, *77* (18), 3865–3868.

- (10) Kresse, G.; Furthmüller, J. Efficient Iterative Schemes for Ab Initio Total-Energy Calculations Using a Plane-Wave Basis Set. *Phys. Rev. B. Condens. Matter* **1996**, *54* (16), 11169–11186.
- (11) Blöchl, P. Projector Augmented-Wave Method. *Phys. Rev. B* **1994**, *50* (24).
- (12) Bergerhoff, G.; Hundt, R.; Sievers, R.; Brown, I. D. The Inorganic Crystal Structure Data Base. *J. Chem. Inf. Model.* **1983**, *23* (2), 66–69.
- (13) Ping Ong, S.; Wang, L.; Kang, B.; Ceder, G. Li–Fe–P–O 2 Phase Diagram from First Principles Calculations. *Chem. Mater.* **2008**, *20* (5), 1798–1807.
- (14) Mills, G.; Jónsson, H. Quantum and Thermal Effects in H₂ Dissociative Adsorption: Evaluation of Free Energy Barriers in Multidimensional Quantum Systems. *Phys. Rev. Lett.* **1994**, *72* (7), 1124–1127.
- (15) Mo, Y.; Ong, S. P.; Ceder, G. First Principles Study of the Li₁₀GeP₂S₁₂ Lithium Super Ionic Conductor Material. *Chem. Mater.* **2012**, *24*, 15–17.
- (16) Marrone, T. J.; Briggs, J. M.; McCammon, J. a. Structure-Based Drug Design: Computational Advances. *Annu. Rev. Pharmacol. Toxicol.* **1997**, *37*, 71–90.
- (17) Ong, S. P.; Richards, W. D.; Jain, A.; Hautier, G.; Kocher, M.; Cholia, S.; Gunter, D.; Chevrier, V. L.; Persson, K. A.; Ceder, G. Python Materials Genomics (pymatgen): A Robust, Open-Source Python Library for Materials Analysis. *Comput. Mater. Sci.* **2013**, *68*, 314–319.
- (18) Ito, S.; Fujiki, S.; Yamada, T.; Aihara, Y.; Park, Y.; Kim, T. Y.; Baek, S. W.; Lee, J. M.; Doo, S.; Machida, N. A Rocking Chair Type All-Solid-State Lithium Ion Battery Adopting Li₂O-ZrO₂ Coated LiNi_{0.8}Co_{0.15}Al_{0.05}O₂ and a Sulfide Based Electrolyte. *J. Power Sources* **2014**, *248*, 943–950.
- (19) Weppner, W.; Hartwig, P.; Rabenau, a. Consideration of Lithium Nitride Halides as Solid Electrolytes in Practical Galvanic Cell Applications. *J. Power Sources* **1981**, *6* (3), 251–259.
- (20) Holzwarth, N. a. W.; Lepley, N. D.; Du, Y. a. Computer Modeling of Lithium Phosphate and Thiophosphate Electrolyte Materials. *J. Power Sources* **2011**, *196* (16), 6870–6876.
- (21) Li, Y.; Zhan, H.; Liu, S.; Huang, K.; Zhou, Y. Electrochemical Properties of the Soluble Reduction Products in Rechargeable Li/S Battery. *J. Power Sources* **2010**, *195* (9), 2945–2949.
- (22) Han, S.-C.; Song, M.-S.; Lee, H.; Kim, H.-S.; Ahn, H.-J.; Lee, J.-Y. Effect of Multiwalled Carbon Nanotubes on Electrochemical Properties of Lithium/Sulfur Rechargeable Batteries. *J. Electrochem. Soc.* **2003**, *150* (7), A889.
- (23) Kamaya, N.; Homma, K.; Yamakawa, Y.; Hirayama, M.; Kanno, R.; Yonemura, M.; Kamiyama, T.; Kato, Y.; Hama, S.; Kawamoto, K.; Mitsui, A. A Lithium Superionic Conductor. *Nat. Mater.* **2011**, *10* (9), 682–686.

- (24) Epp, V.; Gün, Ö.; Deiseroth, H.-J.; Wilkening, M. Highly Mobile Ions: Low-Temperature NMR Directly Probes Extremely Fast Li⁺ Hopping in Argyrodite-Type Li₆PS₅Br. *J. Phys. Chem. Lett.* **2013**, *4* (13), 2118–2123.
- (25) Murugan, R.; Thangadurai, V.; Weppner, W. Fast Lithium Ion Conduction in Garnet-Type Li₇(La₃Zr₂)O₁₂. *Angew. Chem. Int. Ed. Engl.* **2007**, *46* (41), 7778–7781.
- (26) Buschmann, H.; Dölle, J.; Berendts, S.; Kuhn, A.; Bottke, P.; Wilkening, M.; Heitjans, P.; Senyshyn, A.; Ehrenberg, H.; Lotnyk, A.; Duppel, V.; Kienle, L.; Janek, J. Structure and Dynamics of the Fast Lithium Ion Conductor “Li₇La₃Zr₂O₁₂”. *Phys. Chem. Chem. Phys.* **2011**, *13* (43), 19378–19392.

Acknowledgements

The authors would like to thank Samsung Advanced Institute of Technology for funding support on this research. This work used computational resources provided by the Extreme Science and Engineering Discovery Environment (XSEDE), supported by National Science Foundation grant number ACI-1053575, and the National Energy Research Scientific Computing Center (NERSC), a DOE Office of Science User Facility supported by the Office of Science of the U.S. Department of Energy under Contract No. DE-AC02-05CH11231.

Additional information

Electronic supplementary information is available.

$\text{Li}_9\text{S}_3\text{N}$ is a novel Li-metal barrier coating for all-solid-state batteries. The conductivity is greatly improved by Ca_{Li} substitution.

